Cavity phenomena in mesas of cuprate high-T_c superconductors under voltage bias

Xiao Hu[1,2,3] and Shizeng Lin[1,2]
[1]*WPI Center for Materials Nanoarchitectonics, National Institute for Materials Science, Tsukuba 305-0044, Japan*
[2]*Graduate School of Pure and Applied Sciences, University of Tsukuba, Tsukuba 305-8571, Japan*
[3]*Japan Science and Technology Agency, 4-1-8 Honcho, Kawaguchi, Saitama 332-0012, Japan*
(Received 12 March 2009; revised manuscript received 18 June 2009; published 27 August 2009)

Modeling a single crystal of cuprate high-T_c superconductor, such as $Bi_2Sr_2CaCu_2O_{8+\delta}$, as a stack of intrinsic Josephson junctions, we formulate explicitly the cavity phenomenon of plasma oscillations and electromagnetic (EM) waves in mesas of cylindrical and annular shapes. The phase differences of the junctions are governed by the inductively coupled sine-Gordon equations, with the Neumann-type boundary condition for sample thickness much smaller than the EM wavelength, which renders the superconductor single crystal a cavity. Biasing a dc voltage in the *c* direction, a state with $\pm\pi$ kinks in the superconductivity phase difference piled up alternatively along the *c* axis is stabilized. The $\pm\pi$ phase kinks provide interlock between superconductivity phases in adjacent junctions, taking the advantage of huge inductive couplings inherent in the cuprate superconductors, which establishes the coherence across the whole system of more than ~600 junctions. They also permit a strong coupling between the lateral cavity mode of the transverse Josephson plasma and the *c*-axis bias, and enhance the plasma oscillation significantly at the cavity modes which radiates EM waves in the terahertz band when the lateral size of mesa is set to tens of micrometers. It is discussed that the cavity mode realized in a very recent experiment using a cylindrical mesa can be explained by the present theory. In order to overcome the heating effect, we propose to use annular geometry. The dependence of frequency on the radius ratio is analyzed, which reveals that the shape tailor is quite promising for improving the present technique of terahertz excitation. The annular geometry may be developed as a waveguide resonator, mimicking the fiber lasers for visible lights.

DOI: 10.1103/PhysRevB.80.064516 PACS number(s): 74.50.+r, 74.25.Gz, 85.25.Cp

I. INTRODUCTION

The Josephson effect provides a unique principle to excite high-frequency electromagnetic (EM) waves.[1,2] Much effort has been made to stimulate powerful radiations, first using artificial Josephson junction arrays[3–11] and later on Josephson junctions inherent in cuprate high-T_c superconductors of layered structures.[12–26] The latter have obvious advantages since the junctions are homogeneous at the atomic scale guaranteed by the high quality of single crystals, and the superconductivity gap is large, typically of tens of meV, which in principle permits the frequency to cover the whole range of the terahertz (THz) band, a very useful regime of EM waves still lacking of compact solid-state generators.[27,28]

An experimental breakthrough was achieved in 2007.[29] Clear evidences have been obtained that coherent terahertz radiations from side edges of a thin rectangular mesa were realized by biasing a dc voltage in the *c* axis of the $Bi_2Sr_2CaCu_2O_{8+\delta}$ (BSCCO) single crystal; the frequency of the EM wave and the voltage where the radiation occurs obey the ac Josephson relation, and the frequency coincides with one of the cavity modes determined by the lateral size of mesa.[29]

This discovery is expected to leave significant and long-standing impacts. It has the potential to open a practical way to develop a source of frequency tunable EM waves based on superconductivity and fill the so-called THz gap. It also shines light on new directions of making use of the phase of superconductivity. Its importance would be better appreciated if one notices that up to now the usage of superconductivity phase variable is still limited to the superconducting quantum interference device.

The discovery immediately raises many interesting questions, such as why the Josephson plasma oscillation, namely, the coherent tunneling of Cooper pairs back and forth between adjacent CuO layers driven by a *c*-axis voltage, can radiate strong *transverse* radiations in absence of Josephson vortices induced by an applied magnetic field, how it becomes possible to synchronize the superconductivity phase variables of ~600 junctions, and so on. These quests challenge our knowledge on superconductivity as well as nonlinear phenomena in general.

It is formulated explicitly in Ref. 23 that there is a significant mismatch in impedance $|Z_{\rm out}|/|Z_{\rm in}| \sim \lambda_{\rm EM}/L_z$ at the edge of a superconductor mesa when the thickness of the mesa L_z is small compared with the EM wavelength $\lambda_{\rm EM}$, which was known for a single junction as a limiting case.[30] This makes the tangential component of oscillating magnetic field at the mesa edge extremely small compared with the electric one, in sharp contrast to the case of EM plane waves. Actually, this relation is a general property shared by a normal capacitor with small electrode separation. Particularly for thin mesas of superconductor, the vanishingly small tangential component of magnetic field gives the Neumann-type boundary condition of superconductivity phase difference across junctions, namely, the spatial derivative of the phase difference normal to the edge should be zero (in absence of an applied magnetic field).

With this Neumann boundary condition, a new dynamic state of superconductivity phase difference has been found in a stack of Josephson junctions under a dc voltage bias, which is characterized by static $\pm\pi$ [actually $\pm(2m+1)\pi$ with *m* as integer] phase kinks piled up alternatively along the *c* axis[31–33] (see also Ref. 34). In this π kink state, an interlock

between superconductivity phases in neighboring junctions appears, which establishes the coherence across the whole system of more than ~600 junctions. The π phase kink makes the lateral cavity modes of the transverse Josephson plasma couple strongly with the c-axis bias, permits large dc supercurrent flow into the junctions, and generates strong EM radiations from the sides of mesa.

The π kink state requests strong inductive couplings between adjacent superconducting layers,[31] which is guaranteed in the cuprate high-T_c superconductor BSCCO. Another condition is on the thickness of the superconductor mesa: it should be much smaller than the EM wavelength on one hand, which renders the superconductor mesa a cavity, and on the other hand, it should be thick enough to avoid large surface effects. The samples of $L_z \simeq 1$ μm adopted in the experiment[29] satisfy these requests well. The π kink state is stable against other distortions, such as thermal fluctuations, inhomogeneity of physical parameters, and so on.

This work is motivated by two recent experiments on THz radiations from thin mesas of BSCCO single crystals. The first one is a detection of THz radiations from a cylindrical mesa,[35] after the theoretical proposal[32] for verification of the boundary condition taking advantage of the cylindrical geometry. The second one is an observation on EM standing waves in a rectangular mesa,[36] an approach being able to provide direct evidence for cavity resonance. The dependence of the radiation frequency on the sample radius and the distributions of the EM fields and supercurrent revealed in the present work are expected to be able to give a reference for coming experiments and will be helpful in clarifying the mechanism of the THz radiation from intrinsic Josephson junctions. In addition, we propose to use annular geometry, which not only reduces the Joule heating and enhances the leakage of heat but also provides an additional handle for controlling the radiation frequency, both important from a technological point of view.

The remaining part of the present paper is organized as follows. In Sec. II, we discuss the right boundary condition for thin mesas from a theoretical point of view. Then we point out that the result of the recent experiment using a cylindrical mesa is to be understood in accordance with this boundary condition. In Sec. III, a couple of cavity modes possibly available in experiments are presented, with the spatial distributions of the π kink in superconductivity phase difference, supercurrent, as well as the EM standing wave. Section IV is devoted to discussion on annular geometry, which reveals its merits over the cylindrical geometry. Finally summary and perspectives are given in Sec. V.

II. BOUNDARY CONDITION AND CYLINDRICAL MESA

A. Basic equation and general solution

The inductively coupled sine-Gordon equations for the gauge-invariant phase differences in a stack of Josephson junctions with a dc bias and dissipations are given in the dimensionless form as[31–33]

$$\Delta P_l = (1 - \zeta\Delta^{(2)})(\sin P_l + \beta\partial_t P_l + \partial_t^2 P_l - J_{\text{ext}}), \qquad (1)$$

with Δ as the Laplace operator in lateral directions, $\Delta^{(2)}Q_l = Q_{l+1} + Q_{l-1} - 2Q_l$ as the second difference operator along the c axis, $\zeta \equiv \lambda_{ab}^2/d^2 \sim 10^5$ as the inductive coupling (d standing for the period of BSCCO lattice in the c direction), and $\beta \equiv 4\pi\sigma_c\lambda_c/c\sqrt{\varepsilon} = 0.02$ as the c-axis conductivity; the lateral space is scaled by λ_c and time by the inverse of intrinsic plasma frequency $\lambda_c\sqrt{\varepsilon}/c$. For more details of definitions see Refs. 31–33. For a sample of thickness much smaller than the EM wavelength, the Neumann-type boundary condition should be taken for the lateral directions $\partial_n P_l \simeq 0$.

A same set of Eq. (1) was used for stacks of artificial Josephson junctions where superconductor layers are of thickness sufficient for defining a penetration depth. It can also be derived from the Lawrence-Doniach model for cuprate high-T_c superconductors[37,38] (see also Ref. 33). As for the mesa structure of system used in experiments,[29,39] there is no evidence showing that the substrate of BSCCO single crystal plays a crucial role in the phase dynamics in the mesa and the EM radiation. Taking the mesa of large number (~600) of junctions as a bulk system, we neglect the effect from the substrate.

The experimental observation of the cavity relation of radiation frequency[29,39] indicates that standing waves of plasma oscillation have been built in the cavity formed by the mesa, which in turn implies that the oscillating part of the phase difference satisfies the Laplace equation.[31–33] The plasma oscillation should be uniform since the observed radiations are coherent, known as a super-radiation.[29] Without losing generality, the solution to Eq. (1) can be given by

$$P_l(\boldsymbol{r},t) = \omega t + \tilde{P}(\boldsymbol{r},t) + f_l P^s(\boldsymbol{r}), \qquad (2)$$

where the first term accounts for the finite dc bias voltage and the second for plasma oscillation

$$\tilde{P}(\boldsymbol{r},t) = Ag(\boldsymbol{r})\sin(\omega t + \varphi) \qquad (3)$$

with A as the amplitude, $g(\boldsymbol{r})$ as an eigenfunction of the Laplace equation with the Neumann boundary condition, and the frequency given by the voltage following the ac Josephson relation; the third term carries the interjunction coupling via the l dependence.

The general form of Eq. (2) describes a wealth of solutions even giving the constraint imposed by available experimental results. However, it is easy to see[31–33] that the sequences $f_l = (-1)^l$ or $f_l = (-1)^{[l/2]}$ with period two or four layers, respectively, diagonalize Eq. (1) due to the property of the difference operator $\Delta^{(2)}$. In simulations, these two states appear frequently and are stable.[31,33] Here we focus the attention to these two cases.

In an approximation established well for small amplitude A, the phase shift φ is given by

$$\tan\varphi = \beta\omega/(\omega^2 - k^2), \qquad (4)$$

where k is the wave number of cavity mode (see below). The static phase $P^s(\boldsymbol{r})$ and amplitude A should satisfy the following equations:

$$\Delta P^s = \tfrac{1}{2}Aq\zeta\cos\varphi g(\boldsymbol{r})\sin P^s, \qquad (5)$$

with the same Neumann boundary condition, where $q=4$ and 2 for the c-axis sequence of periods 2 and 4, respectively, and

$$A^2 = \frac{1}{(\omega^2 - k^2)^2 + (\beta\omega)^2} \left\{ \frac{\int_\Omega d\boldsymbol{r} g(\boldsymbol{r}) \cos P^s}{\int_\Omega d\boldsymbol{r} [g(\boldsymbol{r})]^2} \right\}^2, \quad (6)$$

with Ω as the lateral cross section of mesa.

The nontrivial solution $P^s(\boldsymbol{r})$ presumes the π phase kink[31–33] (see also Ref. 34). The static c-axis supercurrent which contributes to the net current flowing into the system in the c direction is given by

$$J_s(\boldsymbol{r}) = \tfrac{1}{2} A \sin\varphi g(\boldsymbol{r}) \cos[P^s(\boldsymbol{r})]. \quad (7)$$

The trivial vacua solution $P^s=0$ (Refs. 40–42) is dropped here since the associated solutions are probably unstable near the cavity voltage.[33,43]

It is noticed that harmonics should exist in any cavity phenomena. For sine-Gordon equations, multiples of a cavity frequency intervene with each other. Equation (3) including only a single frequency should be understood as an approximation. The approximation becomes worse close to resonance where the amplitude A is large and thus harmonics should be taken into account. For the rectangular geometry, multiples of a resonating cavity frequency correspond to cavity modes of higher wave numbers. Amplitudes for a resonating frequency and its multiples are enhanced in the same way as indicated in Eq. (6). The ratio of amplitudes for the double frequency and the resonating frequency is therefore of order of 1/2 (see also Ref. 31). However, for the cylindrical geometry, the frequency double of a resonating cavity one does not correspond to a cavity mode since the wave numbers of cavity modes (namely, zeros of derivative of the Bessel function) are not equally separated. According to Eq. (6), the amplitude for the double of the resonating frequency will not be enhanced. The amplitude ratio should then roughly be of order of β. For small conductance such as $\beta = 0.02$ adopted in the present work, typically for high-T_c superconductor BSCCO, the suppression of amplitudes of harmonics is significant compared with the rectangular geometry.

The oscillating electric and magnetic fields inside the junctions are given by the plasma oscillation term of the phase difference in dimensionless forms as

$$E^z(\boldsymbol{r},t) = \frac{\partial \tilde{P}}{\partial t}, \quad (8)$$

with $E^x, E^y \simeq 0$ to a good approximation in cuprates,[31] and

$$\boldsymbol{B}(\boldsymbol{r},t) = -\nabla \times [\tilde{P}(\boldsymbol{r},t)\hat{z}], \quad (9)$$

with $\hat{z}$ as the unit vector in the c axis. It is Eq. (9) that enforces the boundary condition for the phase difference $\partial_n P_l = 0$ with n as the normal of the sample edges.

B. Verification of the boundary condition

In a rectangular mesa, the spatial part of the plasma term of the lowest cavity mode satisfying the right boundary condition is $\cos(x\pi/L)$. Unfortunately, $\cos(x\pi/L)$ and $\sin(x\pi/L)$ are both eigenfunctions of the Laplace equation and give the same wave number (or equivalently frequency in dimensionless form) π/L. Therefore, from a pure experimental point of view, the dependence of frequency on the system size[29] cannot determine uniquely the mode.

Cylindrical geometry was proposed to identify uniquely the dynamics of the superconductivity phase difference inside the junctions.[32] For the cylinder geometry, the radial part of eigenfunction of the Laplace equation is given by the Bessel function. The boundary condition for the cylinder geometry determines uniquely the wave number and vice versa since the zeros of the Bessel functions are different from the zeros of their derivatives, contrasting to sine and cosine functions in the rectangle geometry. Therefore, measuring by experiments the frequency of EM radiation from a cylindrical mesa of given radius and assigning the mode by the properties of Bessel functions enable one to identify uniquely the right boundary condition for the EM waves. It was addressed that, from the boundary condition suitable for thin mesas, the frequency of radiation should be given by the zeros of derivatives of Bessel functions.[32] A mode uniform azimuthally was worked out explicitly, and the frequency is figured out as $k=\chi/a$ with the radius a and $\chi=3.8317$, the first zero of derivative of the Bessel function $J_0(z)$.[44]

A very recent experiment[35] showed that the frequency of EM wave radiated from the cylindrical mesa of radius $a \simeq 45$ μm is $f \simeq 0.474$ THz. With the light velocity in the sample $c' = c/\sqrt{\varepsilon} \simeq 7.16 \times 10^7$ m/s [$\varepsilon \simeq 17.54$ (Ref. 45)], the wave number observed in the experiment[35] is given by $k = \chi/a$ with $\chi \simeq 1.87$, which is close to $\chi = 1.8412$, the first zero of derivative of the Bessel function $J_1(z)$. Therefore, the experiment indicates unambiguously that the frequency of EM radiation is determined by the zero of derivative of the Bessel function, in agreement with the theoretical works.[23,32]

III. MODES FOR CYLINDRICAL MESA

Since the distribution of EM standing wave can be observed directly in experiments[36] and serves as a check of theory, we map it out explicitly for a couple of cavity modes with lowest frequencies for cylindrical geometry. The distributions of superconductivity phase difference and the supercurrent are also presented which are helpful in understanding the way how large dc powers are converted to high-frequency transverse radiations.

The spatial part of the plasma term of (m,n) mode [Eq. (3)] is given by

$$g^c_{mn}(\boldsymbol{r}) = J_m\left(\frac{\chi^c_{mn}}{a}\rho\right)\cos(m\phi) \quad (10)$$

with the cylindrical coordinate $\boldsymbol{r}=(\rho,\phi)$, a as the radius of the cylinder, and χ^c_{mn} as the nth zero of derivative of Bessel function $J_m(z)$ (see Table I). The wave number of each cavity mode is given by $k^c_{mn} = \chi^c_{mn}/a$. For a cylinder with uniform physical properties, the eigenfunction for the azimuthal angle $\sin(m\phi)$ degenerates with $\cos(m\phi)$, which, and any linear combination of them, can be absorbed into the latter by redefining the azimuthal angle ϕ, and will not be discussed explicitly.

TABLE I. Position χ^c_{mn} of the nth zero of the derivative of the Bessel function $J_m(z)$. Factors j^c_{mn}, s^c_{mn}, and e^c_{mn} are defined in Eqs. (11)–(13).

(m,n)	(1,1)	(2,1)	(0,1)	(1,2)
χ^c_{mn}	1.8412	3.0542	3.8317	5.3314
j^c_{mn}	0.3792	0.3452	0.3566	0.3135
s^c_{mn}	1.076	1.209	0.3566	1.181
e^c_{mn}	3.380	3.797	2.241	3.710

A. (1,1) mode

The wave number, or equivalently frequency ($k=\omega$ in dimensionless form and $k=\omega/c'$ with units), of the (1,1) mode for the cylinder $k^c_{11}=\chi^c_{11}/a$ agrees well with the experiment[35] as discussed in Sec. III.

The distribution of the static phase P^s, the supercurrent, and the spatial part of the oscillating electric and magnetic fields are displayed in Fig. 1. The π phase kink runs along the diameter at the direction $\phi=\pm\pi/2$, and the phase saturates to 0 and π at the left and right parts of the cylinder [Fig. 1(a)].

Associated with the static phase kink, the oscillating magnetic field assumes the maximal absolute value along the diameter at $\phi=\pm\pi/2$ and decreases to zero at the leftmost and rightmost parts of the cylinder [Fig. 1(d)]. The azimuthal component of the magnetic field is always zero at the edge of cylinder, as imposed by the boundary condition. The electric field takes its maximal absolute value at the leftmost and rightmost parts, while it is reduced to zero along the diameter at $\phi=\pm\pi/2$ [Fig. 1(c)].

Comparing the distributions of the π phase kink and the electric and magnetic fields, it is found that the (1,1) mode for the cylinder geometry corresponds to the (1,0) mode for the rectangle geometry.[32]

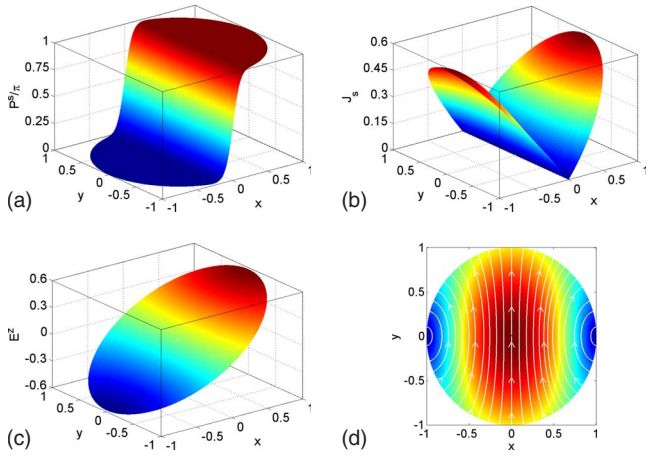

FIG. 1. (Color online) Spatial distribution of (a) the static phase term P^s, (b) the supercurrent, and the standing (c) electric and (d) magnetic waves for the (1,1) mode of a cylindrical mesa. Here $Aq\zeta\cos\varphi=5000$ is taken for Eq. (5) in (a) and the kink is approximated as a step function in (b). The lateral coordinates are normalized by the radius of the cylinder. The quantities except the phase difference P^s are up to the plasma amplitude A.

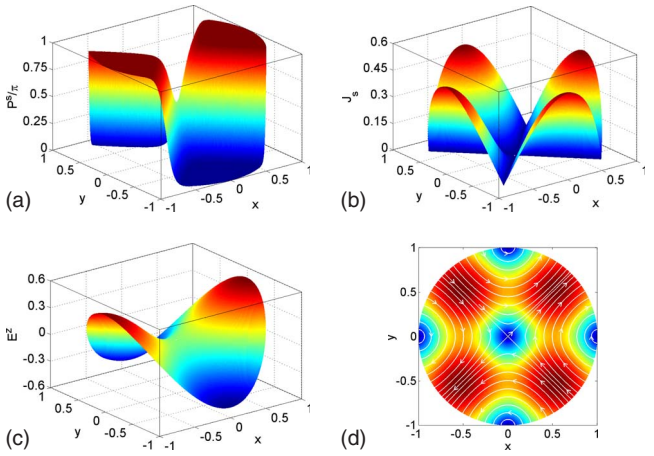

FIG. 2. (Color online) Same as Fig. 1 for the (2,1) mode of a cylindrical mesa.

The maximal value of the supercurrent takes place at the leftmost and rightmost parts of the cylinder for the present mode. The factor $\cos[P^s(\boldsymbol{r})]$ from the π phase kink [Fig. 1(a)] renders the supercurrent associated with the cavity mode $g(\boldsymbol{r})$ positive over the cylinder [Fig. 1(b)] as in Eq. (7), which permits large bias current when the plasma amplitude A is enhanced at the cavity resonance.

B. (2,1) mode

The patterns for the (2,1) mode are displayed in Fig. 2. There are two pairs of $\pm\pi$ kinks in the azimuthal direction [Fig. 2(a)], which increase the frequency to $k^c_{21}=\chi^c_{21}/a$ (see Table I) higher than the (1,1) mode where the π kink running along a diameter [Fig. 1(a)] equivalent to a pair of $\pm\pi$ kinks in the azimuthal direction.

The magnetic field penetrates into the cylinder along two directions [Fig. 2(d)], $\phi=3\pi/4$ and $\phi=-\pi/4$, and flows away along the two orthogonal directions, $\phi=\pi/4$ and $\phi=-3\pi/4$, where the absolute value of magnetic field assumes its maximum. The electric field and the supercurrent become maximal at the directions of multiples of $\phi=\pi$. The (2,1) mode for the cylinder geometry corresponds to the (1,1) mode for the rectangle geometry.[32]

C. (0,1) mode

For comparison, we display in Fig. 3 the patterns for the (0,1) mode for cylinder geometry which has been discussed in Ref. 32. Since this mode is uniform azimuthally, the π phase kink has to be compressed into the radial direction [Fig. 3(a)]. This makes the spatial variation in the magnetic field steep [Fig. 3(d)], and thus the wave number increases to $k^c_{01}=\chi^c_{01}/a$ (see Table I), which is to be excited at a voltage higher than the above (1,1) and (2,1) modes. The magnetic field is circular in this mode [Fig. 3(d)], and in order to match the boundary condition at the edge it is suppressed to zero totally. The magnetic field is also suppressed to zero at the center.

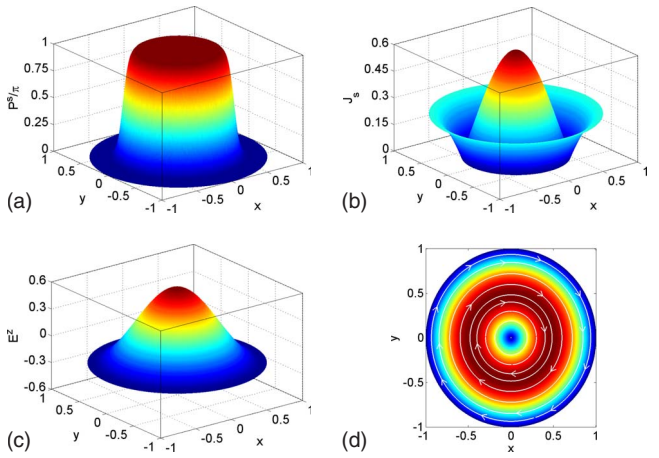

FIG. 3. (Color online) Same as Fig. 1 for the (0,1) mode of a cylindrical mesa.

D. (1,2) mode

The π phase kink can occur simultaneously in both azimuthal and radial directions. The lowest mode of this type is the (1,2) mode (see Table I) shown in Fig. 4.

E. *IV* characteristics

The *IV* characteristics is linear away from the cavity voltage and is given approximately by[31–34]

$$J_{\rm ext} = \beta\omega\left\{1 + \frac{j_{mn}}{[\omega^2 - (\chi_{mn}/a)^2]^2 + (\beta\omega)^2}\right\} \qquad (11)$$

for voltage close to a cavity mode with the factor j_{mn} summarized in Table I for the four lowest cavity modes for cylindrical geometry. It is noticed that the factor j_{mn} does not depend on the radius. In the present approximation, the maximal current at the cavity resonance is $\beta\chi_{mn}/a + j_{mn}/(\beta\chi_{mn}/a)$ in units of J_c, and the Q factor is $\chi_{mn}/(a\beta)$ with a prefactor of order of unity. Since the present approximation fails when A becomes large, the estimate on the maximal current should be interpreted as an upper bound. A

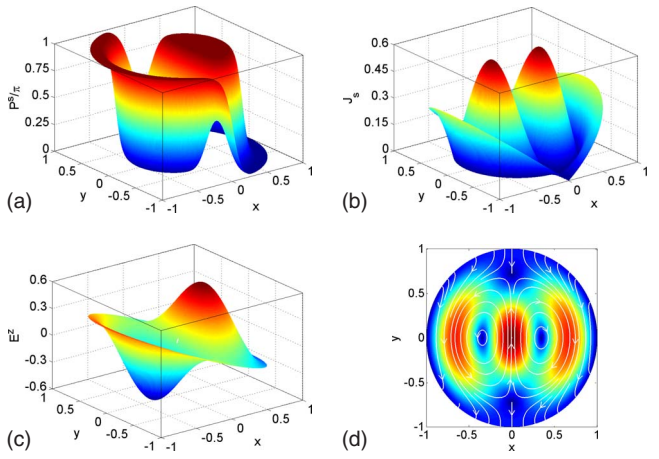

FIG. 4. (Color online) Same as Fig. 1 for the (1,2) mode of a cylindrical mesa.

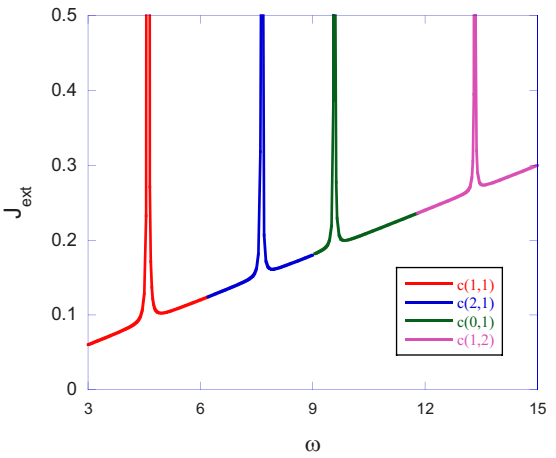

FIG. 5. (Color online) *IV* characteristics for the cylindrical mesa including the four lowest modes. The dimensionless voltage, or equivalently the wave number and frequency, is given by $\omega = \chi^c/a$ with $\chi^c = 1.8412$, 3.0542, 3.8317, and 5.3314 for the (1,1), (2,1), (0,1), and (1,2) modes, respectively. The radius of cylinder is $a = 0.4$ ($a = 0.4\lambda_c$).

treatment with improvement on the peak value of current at the resonance is available for the present cylindrical geometry similar to the rectangular case.[32] In Fig. 5, we display the *IV* characteristics for a cylinder of radius $a = 0.4$.

F. Radiation from cylindrical mesa

The Poynting vector at the perimeter of the cylinder is given by

$$s = \frac{s_{mn}\cos^2(m\phi)/|Z|}{[\omega^2 - (\chi_{mn}/a)^2]^2 + (\beta\omega)^2}, \qquad (12)$$

with Z as the effective surface impedance, and the total energy radiation per unit length in the c axis is given by

$$e = \frac{e_{mn}a/|Z|}{[\omega^2 - (\chi_{mn}/a)^2]^2 + (\beta\omega)^2}, \qquad (13)$$

with the factors s_{mn} and e_{mn} summarized in Table I for the first four cavity modes in the cylindrical geometry.

The radiation pattern of each mode can be computed by using the Huygens principle,[33,46] and the result is displayed in Fig. 6.

IV. ANNULAR MESA

A hurdle for the present technique to excite EM waves of high frequency is the heating effect since the corresponding high dc voltage injects large currents into the sample resulting in severe Joule heating. One way to overcome this effect may be to dig a hole in the superconductor mesa, rendering, for example, a cylindrical one to annular, which reduces the cross section, and thus the total current and Joule heating. Additionally the inner surface of an annular mesa may help leaking heat generated in the mesa. Tailoring the shape of superconductor mesa however will affect the cavity mode and thus the radiation frequency in a nontrivial way. In order

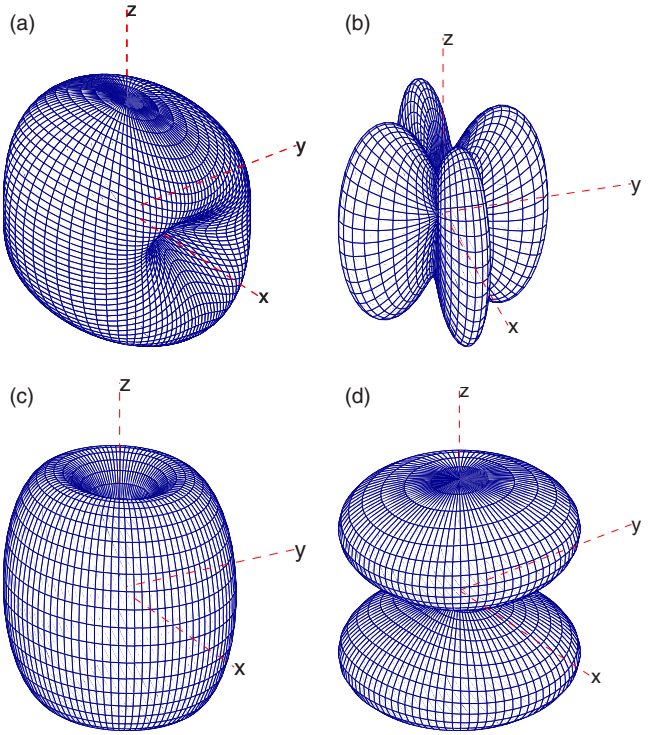

FIG. 6. (Color online) Radiation patterns for (a) (1,1) mode, (b) (2,1) mode, (c) (0,1) mode, and (d) (1,2) mode of cylindrical mesa at the respective resonance frequency. The radius of the mesa is $a=0.4$.

to check this effect, we need to understand the cavity phenomenon for the annular geometry.

For the annular geometry, the spatial part of the plasma term of (m,n) mode is given by

$$g^a_{mn}(\boldsymbol{r}) = \left[J_m\left(\frac{\chi^a_{mn}}{a_o}\rho\right) + pN_m\left(\frac{\chi^a_{mn}}{a_o}\rho\right)\right]\cos(m\phi), \quad (14)$$

where $N_m(z)$ is the Bessel function of second kind and a_o is the outer radius. The Neumann boundary condition should be satisfied at both the outer and inner surfaces. This determines the coefficient χ^a_{mn},

TABLE II. The nth solution χ^a_{mn} of Eq. (15) associated with the Bessel function J_m and N_m for annular sample with $a_i/a_o=1/2$. The factor j^a_{mn} is defined in Eq. (11), $s^{a,i}_{mn}$ and $s^{a,o}_{mn}$ are defined in Eq. (12), and $e^{a,i}_{mn}$ and $e^{a,o}_{mn}$ are defined in Eq. (13) for inner and outer perimeters, respectively.

(m,n)	(1,1)	(2,1)	(0,1)	(1,2)
χ^a_{mn}	1.3546	2.6812	6.3932	6.5649
j^a_{mn}	0.4052	0.4034	0.3964	0.3206
$s^{a,i}_{mn}$	0.7582	0.6160	1.133	1.846
$s^{a,o}_{mn}$	0.8441	0.9385	0.5805	0.9208
$e^{a,i}_{mn}$	2.382	1.935	7.117	5.798
$e^{a,o}_{mn}$	2.652	2.948	3.647	2.893

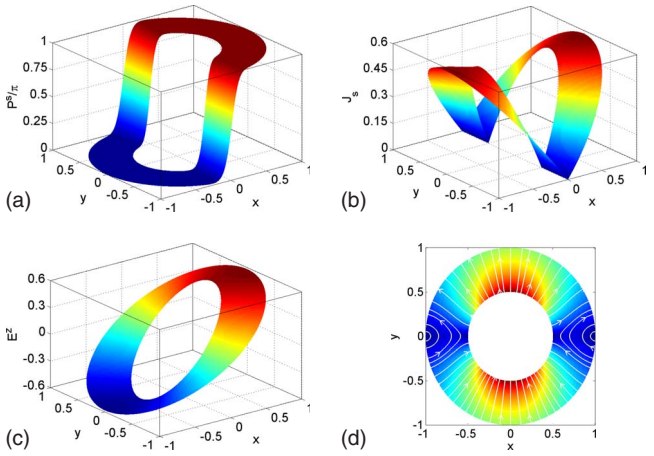

FIG. 7. (Color online) Same as Fig. 1 for the (1,1) mode of an annular mesa except that the lateral coordinates are normalized by the outer radius and the ratio between the inner and outer radii is 1/2.

$$J'_m\left(\chi^a_{mn}\frac{a_i}{a_o}\right)N'_m(\chi^a_{mn}) - J'_m(\chi^a_{mn})N'_m\left(\chi^a_{mn}\frac{a_i}{a_o}\right) = 0, \quad (15)$$

as a function of the ratio a_i/a_o between the inner and outer radius, where $J'_m(z)$ and $N'_m(z)$ are the first derivatives (see Table II). The wave number, or equivalently the frequency, is given by $k^a_{mn}=\chi^a_{mn}/a_o$. The coefficient p in Eq. (14) is then determined by

$$p = -J'_m(\chi^a_{mn})/N'_m(\chi^a_{mn}). \quad (16)$$

A. (1,1) mode

The distributions of the static phase kink, the supercurrent, and the spatial part of the oscillating electric and magnetic fields for (1,1) mode are displayed in Fig. 7 for the case of $a_i/a_o=1/2$. There are two features concerning the redistribution of magnetic field, comparing Figs. 1(d) and 7(d). First, the maximum of magnetic field at the cylinder center is suppressed. Second, the magnetic field becomes along the radial direction in most part of the mesa when the center of mesa is removed since the magnetic field should be normal to both outer and inner surfaces. Both of these two factors suppress the strength of magnetic field and thus reduce the frequency.

B. (2,1) mode

The patterns for the (2,1) mode are displayed in Fig. 8, which is to be compared with Fig. 2. Similar to (1,1) mode, the magnetic field becomes along the radial direction in most part of the mesa.

C. (0,1) mode

The patterns for the (0,1) mode are displayed in Fig. 9. In contrast to the modes (1,1) and (2,1), the magnetic field is circular in the (0,1) mode. The system arranges the magnetic field to zero totally at the two surfaces in order to satisfy the

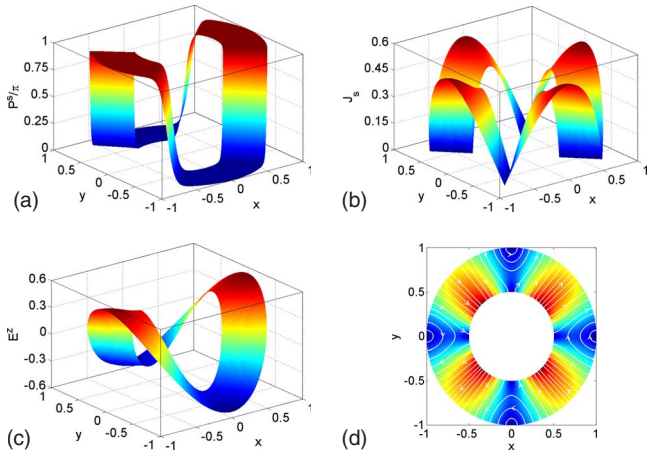

FIG. 8. (Color online) Same as Fig. 7 for the (2,1) mode of an annular mesa.

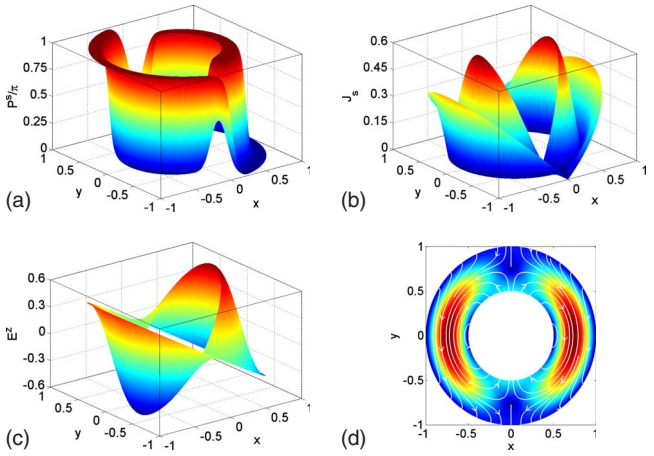

FIG. 10. (Color online) Same as Fig. 7 for the (1,2) mode of an annular mesa.

Newmann boundary condition. Thus, the density of magnetic flux increases when the center of cylinder is removed, which results in a higher frequency.

D. (1,2) mode

The patterns for the (1,2) mode are displayed in Fig. 10. There are two features in the redistribution of magnetic field for this mode as displayed in Fig. 10(d). The maximum of magnetic field at the center of the cylindrical mesa disappears [Fig. 4(d)], similar to (1,1) mode. On the other hand, the density of magnetic flux increases at the other two maxima of magnetic field, similar to (0,1) mode.

E. Dependence of frequency on aspect ratio

The dependence of wave number, or equivalently frequency, on the aspect ratio a_i/a_o is shown in Fig. 11. For the (1,1) and (2,1) modes, the wave number $k^a=\chi^a/a_o$ decreases with increasing ratio a_i/a_o, whereas an opposite trend is seen for the (0,1) mode. The behavior of the (1,2) mode is a compromise of the both trends, yielding a minimum in wave number at $a_i/a_o \simeq 0.2$. These behaviors are well understood from the redistribution of magnetic field in the corresponding cavity modes discussed above.

For the (1,2) mode, the regime $0 \leq a_i/a_o \leq 0.4$ can be used to suppress the Joule heating without changing much the radiation frequency. Since the curves for the (1,1) and (2,1) modes in Fig. 11 are quite flat, they can also be useful for the same purpose. The mode (0,1) and the mode (1,2) with $a_i/a_o > 0.4$ can be used to increase the radiation frequency provided the heating effect can be controlled.

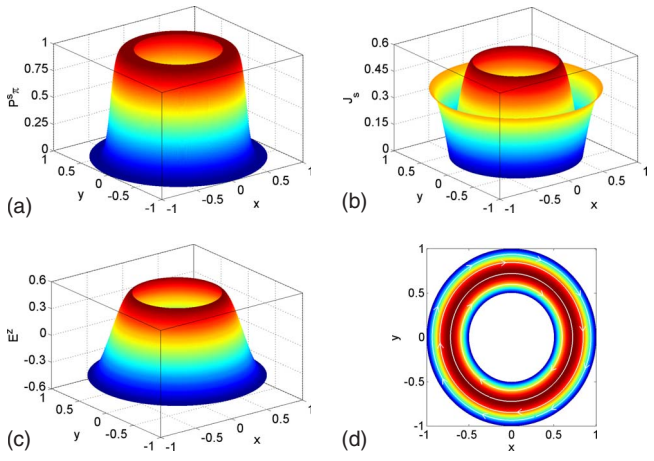

FIG. 9. (Color online) Same as Fig. 7 for the (0,1) mode of an annular mesa.

F. *IV* characteristics

The *IV* characteristics for the annular mesa is also given by Eq. (11), with the factor j_{mn} summarized in Table II for the annular mesa with $a_i/a_o = 1/2$ and displayed in Fig. 12.

G. Radiation from annular mesa

The Poynting vectors at the inner and outer perimeters of the annular sample are given by Eq. (12), with a standing for

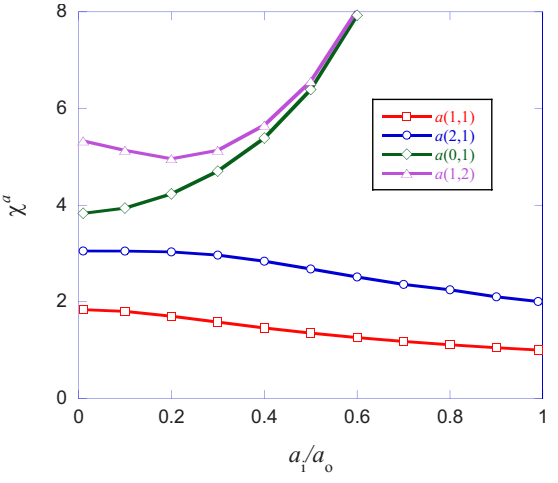

FIG. 11. (Color online) χ^a as a function of the radius ratio a_i/a_o for the lowest four modes for the annular geometry.

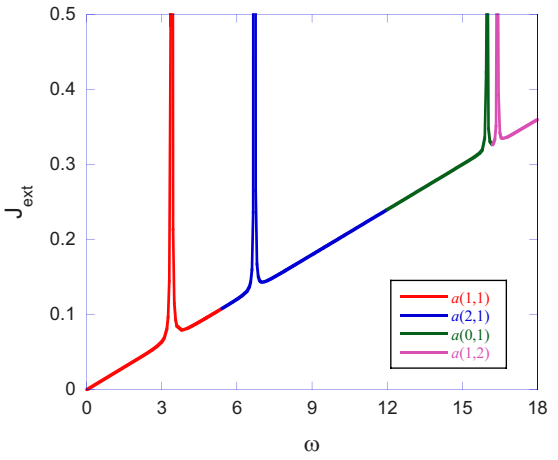

FIG. 12. (Color online) *IV* characteristics for the annular mesa including the four lowest modes. The dimensionless voltage is $\omega = \chi^a / a_o$ with $\chi^a = 1.3546$, 2.6812, 6.3932, and 6.5649 for the (1,1), (2,1), (0,1), and (1,2) modes, respectively. The radius ratio is $a_i / a_o = 1/2$ and outer radius is $a_o = 0.4$.

the outer radius. The factors $s_{mn}^{a,i}$ and $s_{mn}^{a,o}$ are summarized in Table II for $a_i / a_o = 1/2$. The total energy radiations at the inner and outer perimeters per unit length in the c axis are given by Eq. (13), with a in the numerator for the inner and outer radii, respectively, while that in denominator for the outer radius. The factors $e_{mn}^{a,i}$ and $e_{mn}^{a,o}$ are summarized in Table II for $a_i / a_o = 1/2$. The radiation power depends on the aspect ratio a_i / a_o, which can be used to optimize the sample shape.

The radiation pattern of each mode is displayed in Fig. 13 for the annular geometry, where multireflections at the inner radius have been neglected since the mesa thickness is very small compared with the EM wavelength.

V. SUMMARY AND PERSPECTIVES

We first address that the radius dependence of radiation frequency observed in a recent experiment using a cylindrical mesa[35] is to be understood as a clear indication of the Neumann-type boundary condition for mesa of small thickness compared with the EM wavelength, which the π kink state has been derived uniquely for inductively coupled Josephson junctions. Detailed spatial distributions of the superconductivity phase difference with a π phase kink are presented for various cavity modes of cylindrical mesa. Along with them, we also summarize the spatial distribution of the EM standing waves inside the junctions which hopefully can be observed in experiments.

We propose to use annular geometry to excite THz EM radiations. The obvious advantage of the annular geometry is the reduction in heating since the area of sample is reduced

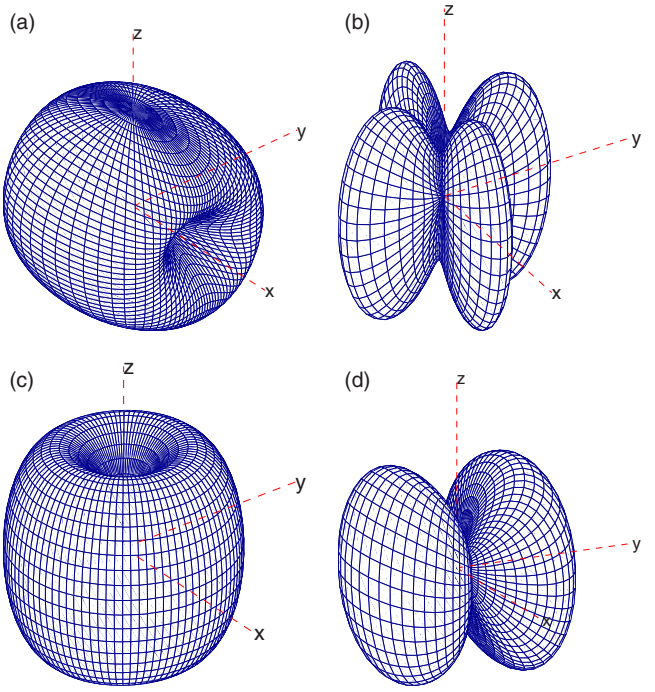

FIG. 13. (Color online) Same as Fig. 6 for annular mesa. Multireflections due to the inner surface are neglected since the thickness of annular mesa is very small compared with the EM wavelength. The radii are $a_i = 0.2$ and $a_o = 0.4$.

which suppresses the total Joule heating and the inner surface of the sample may enhance heat leakage additionally. The effect of removing the central part of a cylindrical mesa, thus rendering an annular one, on the redistribution of the superconductivity phase difference, the supercurrent, and the EM waves is analyzed. It is shown that the radiation frequency varies with the aspect ratio in different ways for different modes, and there is plenty of room for modification of the EM radiation by tailoring the shape of sample while keeping low heating.

Single crystal of superconductor manufactured in annular geometry can also work as a waveguide resonator (see, for example, Ref. 47). In contrast with the fiber lasers developed for visible lights, the lasing mode propagates along the annular superconductor. When the outer surface is shielded by wrapping a jacket made of appropriate materials, new kink state of superconductivity phase can be realized which enhances the electromagnetic wave propagating in the waveguide.

ACKNOWLEDGMENTS

This work was supported by WPI Initiative on Materials Nanoarchitectonics, MEXT of Japan and by CREST, JST and partially by ITSNEM of CAS.

[1] B. D. Josephson, Phys. Lett. **1**, 251 (1962).
[2] A. Barone and G. Paterno, *Physics and Applications of the Josephson Effect* (Wiley, New York, 1982).
[3] I. K. Yanson, V. M. Svistunov, and I. M. Dmitrenko, Zh. Eksp. Teor. Fiz. **48**, 976 (1965).
[4] A. H. Dayem and C. C. Grimes, Appl. Phys. Lett. **9**, 47 (1966).
[5] J. E. Zimmerman, J. A. Cowen, and A. H. Silver, Appl. Phys. Lett. **9**, 353 (1966).
[6] N. F. Pedersen, O. H. Soerensen, J. Mygind, P. E. Lindelof, M. T. Levinsen, and T. D. Clark, Appl. Phys. Lett. **28**, 562 (1976).
[7] T. F. Finnegan and S. Wahlsten, Appl. Phys. Lett. **21**, 541 (1972).
[8] A. K. Jain, K. K. Likharev, J. E. Lukens, and J. E. Sauvageau, Phys. Rep. **109**, 309 (1984).
[9] A. V. Ustinov, H. Kohlstedt, M. Cirillo, N. F. Pedersen, G. Hallmanns, and C. Heiden, Phys. Rev. B **48**, 10614 (1993).
[10] M. Darula, T. Doderer, and S. Beuven, Supercond. Sci. Technol. **12**, R1 (1999).
[11] P. Barbara, A. B. Cawthorne, S. V. Shitov, and C. J. Lobb, Phys. Rev. Lett. **82**, 1963 (1999).
[12] R. Kleiner, F. Steinmeyer, G. Kunkel, and P. Müller, Phys. Rev. Lett. **68**, 2394 (1992).
[13] S. Sakai, P. Bodin, and N. F. Pedersen, J. Appl. Phys. **73**, 2411 (1993).
[14] M. Tachiki, T. Koyama, and S. Takahashi, Phys. Rev. B **50**, 7065 (1994).
[15] T. Koyama and M. Tachiki, Solid State Commun. **96**, 367 (1995).
[16] S. E. Shafranjuk and M. Tachiki, Phys. Rev. B **59**, 14087 (1999).
[17] E. Kume, I. Iguchi, and H. Takahashi, Appl. Phys. Lett. **75**, 2809 (1999).
[18] R. Kleiner, T. Gaber, and G. Hechtfischer, Phys. Rev. B **62**, 4086 (2000).
[19] I. Iguchi, K. Lee, E. Kume, T. Ishibashi, and K. Sato, Phys. Rev. B **61**, 689 (2000); K. Lee, W. Wang, I. Iguchi, M. Tachiki, K. Hirata, and T. Mochiku, *ibid.* **61**, 3616 (2000); I. Iguchi, E. Kume, and H. Takahashi, *ibid.* **62**, 5370 (2000).
[20] I. E. Batov, X. Y. Jin, S. V. Shitov, Y. Koval, P. Müller, and A. V. Ustinov, Appl. Phys. Lett. **88**, 262504 (2006).
[21] L. N. Bulaevskii and A. E. Koshelev, Phys. Rev. Lett. **97**, 267001 (2006).
[22] L. N. Bulaevskii and A. E. Koshelev, J. Supercond. Novel Magn. **19**, 349 (2006).
[23] L. N. Bulaevskii and A. E. Koshelev, Phys. Rev. Lett. **99**, 057002 (2007).
[24] M.-H. Bae, H.-J. Lee, and J.-H. Choi, Phys. Rev. Lett. **98**, 027002 (2007).
[25] A. E. Koshelev and L. N. Bulaevskii, Phys. Rev. B **77**, 014530 (2008).
[26] S.-Z. Lin, X. Hu, and M. Tachiki, Phys. Rev. B **77**, 014507 (2008).
[27] B. Ferguson and X.-C. Zhang, Nature Mater. **1**, 26 (2002).
[28] M. Tonouchi, Nat. Photonics **1**, 97 (2007).
[29] L. Ozyuzer, A. E. Koshelev, C. Kurter, N. Gopalsami, Q. Li, M. Tachiki, K. Kadowaki, T. Yamamoto, H. Minami, H. Yamaguchi, M. Tachiki, K. E. Gray, W.-K. Kwok, and U. Welp, Science **318**, 1291 (2007).
[30] D. N. Langenberg, D. J. Scalapino, B. N. Taylor, and R. E. Eck, Phys. Rev. Lett. **15**, 294 (1965).
[31] S.-Z. Lin and X. Hu, Phys. Rev. Lett. **100**, 247006 (2008).
[32] X. Hu and S.-Z. Lin, Phys. Rev. B **78**, 134510 (2008).
[33] S.-Z. Lin and X. Hu, Phys. Rev. B **79**, 104507 (2009).
[34] A. E. Koshelev, Phys. Rev. B **78**, 174509 (2008).
[35] K. Kadowaki *et al.* (private communication).
[36] H. B. Wang, S. Guénon, J. Yuan, A. Iishi, S. Arisawa, T. Hatano, T. Yamashita, D. Koelle, and R. Kleiner, Phys. Rev. Lett. **102**, 017006 (2009).
[37] L. N. Bulaevskii, D. Dominguez, M. P. Maley, A. R. Bishop, and B. I. Ivlev, Phys. Rev. B **53**, 14601 (1996).
[38] A. E. Koshelev and I. Aranson, Phys. Rev. B **64**, 174508 (2001).
[39] K. Kadowaki, H. Yamaguchi, K. Kawamata, T. Yamamoto, H. Minami, I. Kakeya, U. Welp, L. Ozyuzer, A. E. Koshelev, C. Kurter, K. E. Gray, and W.-K. Kwok, Physica C **468**, 634 (2008).
[40] H. Matsumoto, T. Koyama, and M. Machida, Physica C **468**, 654 (2008).
[41] T. Koyama, H. Matsumoto, M. Machida, and K. Kadowaki, Phys. Rev. B **79**, 104522 (2009).
[42] M. Tachiki, S. Fukuya, and T. Koyama, Phys. Rev. Lett. **102**, 127002 (2009).
[43] S.-Z. Lin and X. Hu, arXiv:0903.5110 (unpublished).
[44] In most literatures, the first zero in the derivative of Bessel function $J_0(z)$ is set as 3.8317. The better description is to set 0 as the first zero, 3.8317 as the second, and so on so forth. The mode shown in Fig. 3 (see also Ref. 32) would then be assigned as the (0,2) mode in cylinder. The redefined mode (0,1) is the uniform solution, which is not a real cavity mode (Ref. 33).
[45] K. Kadowaki *et al.* (unpublished).
[46] W. L. Stutzman and G. A. Thiele, *Antenna Theory and Design* (Wiley, New York, 1998).
[47] Hamamatsu Photonics K. K. Laser Group, Nature Photonics, Sample Issue, 14, 2006.